IOPscience iopscience.iop.org

Home Search Collections Journals About Contact us My IOPscience

Local density of states in amorphous Ni-P alloys

This article has been downloaded from IOPscience. Please scroll down to see the full text article.

1992 J. Phys.: Condens. Matter 4 2487

(http://iopscience.iop.org/0953-8984/4/10/013)

View the table of contents for this issue, or go to the journal homepage for more

Download details:
IP Address: 171.66.16.159
The article was downloaded on 12/05/2010 at 11:28

Please note that terms and conditions apply.

J. Phys.: Condens. Matter 4 (1992) 2487–2503. Printed in the UK

Local density of states in amorphous Ni–P alloys

J Kojnok†¶, A Szasz†, W Krasser‡, G Mark§, V S Stepanjuk‖ and A A Katsnelson‖

† Laboratory of Surface and Interface Physics, Eotvos University, Budapest Muzeum krt. 6-8, H-1088 Hungary

‡ Forschungszentrum, IFF, Jülich, W-1930, Federal Republic of Germany

§ Technical University, Budapest, Budafoki ut 8, H-1111 Hungary

‖ Moscow State University, Moscow, Lenin Hills, Russia

Received 3 May 1991, in final form 22 October 1991

Abstract. The electronic density of states around the P and Ni atoms in amorphous alloys Ni_xP_{1-x} for different x ($0.08 < x < 0.26$) is investigated using x-ray emission. The Ni d band of the alloy is shifted to higher binding energies by 0.2 eV with respect to that of the pure Ni. The P 3s band becomes more localized and strongly bonded at a binding energy of −13.1 eV. The P 3p band is hybridized with the Ni d band and forms bonding and antibonding bands. The antibonding p band is located at +6.4 eV above the Fermi level, whereas the bonding p band is at −5.9 eV. The d densities of states around the P atoms show special features with respect to those in pure P. These new P d states (at −2.5 eV binding energy, including 0.3 d electrons) come from Ni d states. An amount of 0.3–0.4 electrons (per P atom) is transferred from the Ni atoms to P. This charge transfer corresponds to 0.1 electron per Ni atom. The experimental results have been confirmed by two types of local density calculation using either a cluster approximation or an infinite periodic lattice model where a definite number of Ni atoms are substituted by P impurities. Both computational methods characterize well the measured local and partial density of states.

1. Introduction

The Ni–P system is an excellent model system for studying transition-metal–metalloid glasses. It can easily be prepared using different simple techniques. It is very stable in the easy glass-forming range of 8–26 at.% P range, where it shows interesting physical properties such as a ferromagnetic-to-paramagnetic phase transition at about 18 at.% P [1]. The temperature coefficient of resistance changes from a positive to a negative value above 22 at.% P [2].

The electronic, optic, magnetic and transport properties of the glassy metal–metalloid system are mainly determined by the density of states (DOS) at the Fermi energy, namely $N(E_F)$.

Several experimental methods, such as specific heat [3, 4], Knight shift [5], magnetic measurements [6] and x-ray absorption near-edge spectroscopy [7] have been performed on $Ni_{1-x}P_x$ glasses to determine $N(E_F)$. The main contribution to the DOS results from

¶ Present address: Forschungszentrum Jülich, Institut für Festkörperforschung D-5170 Jülich, Pf 1913, Federal Republic of Germany.

0953-8984/92/102487 + 17 $04.50 © 1992 IOP Publishing Ltd

the metal d states at E_F. Therefore, up to now the main interest was focused on the investigation of the metal d DOS. In the present paper our interest is concentrated onto the features of the metalloid DOS for different metalloid concentrations. It will be shown that the phosphorus DOSs are sensitive to the alloying process.

Several theoretical calculations using different techniques have been developed to determine the electronic structures of this system [8–12]. Considering the charge transfer and the metalloid partial DOS there exist discrepancies between the calculation and the spectroscopic data.

Apart from the rigid-band model, there exist two concurrent interpretations for the concentration dependence of $N(E_F)$. One of them has been presented by Jaswal [8]. For the electronic structure calculations, he used a self-consistent spin-polarized linear-muffin-tin-orbital (LMTO) method. His calculations suppose strong $N(E_F)$ reduction with increasing P concentration assuming a strong charge transfer (0.48 e^- per Ni) from P to Ni. The other model was developed by Ching [9], predicting only a weak concentration dependence of $N(E_F)$ and just an opposite and small (0.13 e^- per Ni) charge transfer. He used an orthogonalized linear combination of atomic orbits applied to a cluster size of 100 atoms. His results were confirmed by Press *et al* [10] with a cluster discrete-variational method.

In our present paper, x-ray emission spectroscopy (XES) in combination with x-ray absorption spectroscopy (XAS) [25] are applied, in order to measure the local electronic distributions which are essentially proportional to the local DOS around the Ni and the P atoms. We have used XPS data to determine the location of the Fermi level [25].

These experimental results are compared with calculations of the DOS, using two different approximations. The DOS is either calculated with a cluster local-coherent-potential approximation (LCPA) or with a linearized augmented-plane-wave (LAPW) approximation which is applied to an infinite Ni matrix with P impurities using the Kohn–Korringa–Rostoker (KKR) muffin-tin potential in each case.

2. Experimental procedure

The XES measurements were performed using a grating mirror spectrometer for the soft-x-ray range [13]. The crystal vacuum spectrometer is equipped with different curved crystals for the higher-energy regime [14]. The Ni $M_{2,3}$ and the P $L_{2,3}$ spectra were excited by electron bombardment in the soft-x-ray range, whereas the Ni $L_{2,3}$ and Ni Kβ and the P Kβ emission spectra were fluorescently excited by Cu Kα source. The parameters of the measurements are collected in tables 1 and 2.

The investigated samples were electroless binary NiP layers with a thickness in the range of 0.1–2.0 μm deposited on Cu, Ni and Fe substrates. Details concerning the sample preparation have been given elsewhere [15]. The phosphorus concentrations were determined from the Ni Kα-to-P Kα intensity ratio [16], without corrections with respect to self-absorption. (Thus, the accuracy of the phosphorus concentration is assumed to be ± 1 at.% P.)

The amorphicity of the samples was checked by x-ray diffraction (XRD). The initially homogeneous and amorphous samples, after annealing at 400 °C are decomposed into two phases. This two phase system is crystalline, consisting of α-Ni and Ni_3P. Nevertheless, no crystallization was observed by XRD during low-intensity electron bombardment with an electric current density in the range of 1 mA mm^{-2}. However, using

Table 1. The main experimental parameters of XES measurements: the characteristic data of the excited lines.

Line	X-ray source	Analyser	Resolution[a] ΔE (eV)	Core splitting (eV)	Core broadening (eV)
Ni $M_{2,3}$	e^-	Grating	0.2	1.0 ($3p_{1/2}$–$3p_{3/2}$)	1.7 [51, 52]
P $L_{2,3}$	e^-	Grating	0.25	0.85 ($2p_{1/2}$–$2p_{3/2}$)	0.1 [52]
Ni L_3	Fluorescence	Beryl crystal	0.15	—	0.7 [53, 54, 58] 0.9 [52] 0.3 [55]
Ni L_3 absorption [56]			0.15		—
P $K\beta$	Fluorescence	Quartz crystal	0.3	—	0.48 [57]
P K absorption [57]			0.3	—	1.0 [44]
Ni $K\beta$	Fluorescence	Quartz[b] LiF crystal	2.8	—	1.2 [51] 1.6 [52]

[a] Theoretical resolution calculated from $\Delta E = 12398.1 \times 2dS\ \cot(\Omega)/(R/\lambda^2)$, where $2d$ is the lattice parameter, S the slit size, Ω the diffraction angle and λ the wavelength.
[b] Quartz $10\bar{1}1$ fourth-order reflection; LiF 200 second.order reflection.

Table 2. The characteristic data of the measured transitions of Ni–P.

Spectrum	I_{max} (eV)	HBW_{exp} (eV)	HBW_{eff}[a] (eV)
Ni $M_{2,3}$	64.8	3.4	1.7 (d band)
P $L_{2,3}$	116.5	4.0	2.8 (3s core)
	127.1	5.0	3.8 (d band)
Ni L_3	851.5	2.55	1.7 (d band)
Ni L_3 absorption [56]	852.5	—	—
P $K\beta$	2137.2	4.5	3.7 (p band)
	2141.6		(peaks S)
P K absorption [31]	2143.7	—	
Accuracy	±0.2	±0.1	±0.2

[a] HBW_{eff} is the calculated effective bandwidth: $HBW_{eff} = HBW_{exp}$ – (resolution broadening).

higher current densities of the excitation beam (above 10 mA mm^{-2}), partial crystallization was detected.

3. Calculation procedures

Two different approximations were used to determine the local and partial DOSs of electrons, with angular momentum $l = 0, 1, 2$ around the Ni and P atoms. The procedures of calculations are based both on a cluster model with a finite number of atoms forming a cluster [17] and on an impurity method, which is applied to an infinite ordered metal, where the host atoms are partially substituted by impurities [18].

The results of the cluster model depend on the size effect and on the boundary conditions as well. On the contrary, the impurity model can overcome the boundary problem and the finite-size effects but gives accurate results only in the dilute limit.

(i) For the cluster calculations, a KKR muffin-tin potential was used. We have applied the Green function formalism with a LCPA in the local-density approximation [17]. Using this method, the electron structure even in random and amorphous structures can be estimated. In our calculations we have assumed a chemical short-range order using both FCC and Ni_3P structures [20]. With respect to this assumption, chemical bonding, hybridization and localization effects may be well described. The initial electron configuration in our model is Ni $3d^{9.4}4s^{0.6}$, P $3s^23p^3$ [19]; the muffin-tin parameters are presented in the appropriate figures. The cluster calculations were extended to the third coordination shell (the largest cluster size is 29 atoms). Note that we must take into consideration the fact that the cluster calculations are not self-consistent with respect to the charge transfer.

(ii) The impurity model calculations are based on a self-consistent KKR Green function muffin-tin method using a linear combination of augmented plane waves (LAPW) [12, 18]. This method can be applied to periodic lattices with long-range order. The applied symmetries are FCC, BCC and simple cubic, but only the FCC results are presented here, because the other results do not agree with the measured Ni or P DOS. Starting from an infinite ordered crystalline Ni lattice, a phosphorus atom is introduced as a perturbation and first-order perturbation theory is applied. The Green function of the original unperturbed state was obtained by the LAPW method. The applied approximation is valid if the impurity–impurity interactions are negligible. With respect to the Ni–P system, this approximation can still be used even to such high P concentrations as about 25 at.%, where the direct P–P interactions are very weak (the P–P effective pair interaction is one third of the corresponding Ni–P interaction [21]). This is confirmed on the Ni_3P, $Ni_{12}P_5$ and Ni_2P structure, where P sites exist with only nearest-neighbour Ni atoms (usually nine) [20]. In this approximation the calculation of the DOS is much more precise around P impurities than around the host Ni.

4. Results and discussion

The total and partial (s, p, d) DOSs are measured and calculated at the Ni and P sites. The XES and XAS spectra of Ni and P are presented in figures 1 and 2. It is well known [22], that the $M_{2,3}$ and L_3 emission spectra contain information on the s and d partial DOSs (assuming that the transition probability of the emission depends only weakly on the bonding energy). On the x-ray energy scale the Fermi level can be positioned according to the binding energy values measured by XPS, as shown in tables 3 and 4 for Ni and P, respectively.

The Ni $M_{2,3}$ and L_3 spectra have mainly a d character. There exists a small contribution from the Ni s DOS, which overlaps with the d states. Moreover the Ni $4s \rightarrow 3p$ x-ray transition probability is much less than the $3d \rightarrow 3p$ transition probability [40] and therefore it is difficult to observe the Ni s states.

On the contrary, the P $L_{2,3}$ spectra show two well separated subbands (peaks) as presented in figure 2. In this case the s (peak A) and d subbands (peak B) are well separated and do not overlap each other considerably; the transition probabilities do not differ strongly [40].

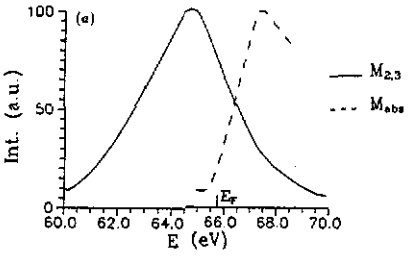

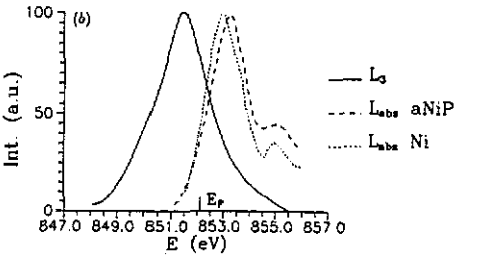

Figure 1. (*a*) The Ni $M_{2,3}$ XES spectra and Ni M absorption [59] spectra of Ni (or Ni–P). (*b*) The Ni $L_{2,3}$ XES spectra and Ni L absorption [56] spectra of Ni (or Ni–P).

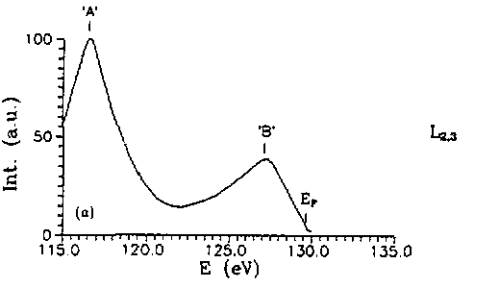

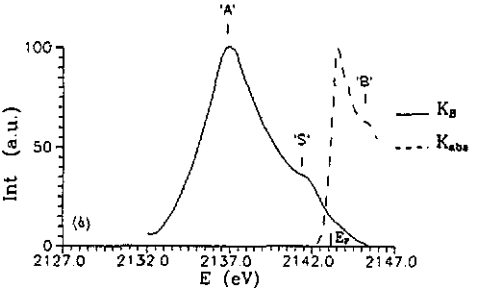

Figure 2. (*a*) The P $L_{2,3}$ XES spectra of Ni–P. (*b*) The P Kβ XES spectra and P K absorption spectra [31] of Ni–P.

Table 3. Ni binding energies in Ni and Ni–P.

	Ni binding energy (eV) in the following			
	$2p_{3/2}$		$3p_{3/2,1/2}$[a]	
Methods	Ni	NiP	Ni	NiP
XPS	852.3 [46]			
	852.6 [32]	852.6 [32]	65.7 [28]	
	852.8 [25]	852.8 [25]		
		852.9[b] [27]		
	852.6 [24]	852.7 [24]		
XES[c]	851.5 + Δ [47]	851.5 + Δ′ [47]	64.8 + δ [47]	64.8 + δ′ [47]
	851.5 + Δ [25]	851.5 + Δ′ [25]	65.0 + δ [48]	
	851.2 + Δ [58]			
XAS		+0.4 shift [7]	66.0 [48]	
	852.2 [25]	852.5 [25]		
Used	852.2	852.4		

[a] Unresolved splitting (1.0 eV).

[b] $Fe_{40}Ni_{40}P_{14}B_6$.

[c] Binding energy calculated from $E_{bind} = E^{XES}_{max} + \Delta$. ($\Delta$ and δ) are energy difference ($E_F - E_{maximum}$) ($\Delta_{Ni} = 0.7 \pm 0.2$ eV; $\Delta_{Ni-P} = 0.9 \pm 0.2$ eV).

Table 4. P binding energies in P and Ni–P.

	P binding energy (eV) in the following			
	1s		$2p_{1/2,3/2}$[a]	
Method	P	NiP	P	NiP
XPS		2143.8 [25]	130.1 [25] 130.1 [31] 129.9 [32]	129.3 [25] 129.7 [31] 129.4 [32] 129.4[b] [27]
XES[c]	2143.0 [25]	2143.0 [25] 2143.6 [25] 2143.1 [47]	130.0 [49]	 129.5 [25] 129.6 [47]
	2142.8 [44]			
XAS	2142.9 [31] 2141.0 [44]	2142.8 [31]	137.0 [50]	

[a] Unresolved splitting (0.8 eV).
[b] $Fe_{40}Ni_{40}P_{14}B_6$.
[c] Binding energies calculated from the Kβ, $L_{2,3}$ spectra using the assumption that E_F is on the top of the spectra.

The Kβ spectra in principle correspond to the energy distribution of the p states. The Ni Kβ spectrum is not presented, because the Ni 3p contribution to the total DOS is very small and the binding energy of the Ni 1s level is very large, which yields a strong core broadening and the instrumental resolution also deteriorates (table 2). Therefore, the P Kβ has been discussed only.

4.1. Density of states around Ni

4.1.1. d band. UPS measurements on binary Ni–P alloys [23] indicate that the d-band structure is quite similar to that of pure Ni. The shift of the Ni–P d band is not clearly resolved within a 0.2 eV resolution.

A shift in the Ni $2p_{3/2}$ core level of about 0.1 eV to higher energies is observed by XPS on amorphous Ni–P alloy [24]. This shift is assumed to be caused by a small charge transfer from Ni to P.

The XES Ni L_3 spectra of pure Ni and amorphous Ni–P are identical within the experimental resolution, but the L_3 absorption edge of Ni–P moves to higher energies with respect to that for pure Ni by 0.3 ± 0.2 eV [25]. From this experimental evidence we have concluded that the d band has been shifted to lower energies with respect to E_F of about 0.2 eV (table 3). This conclusion is in qualitative agreement with the XES results of Tanaka *et al* [26] on amorphous Ni–Si and Ni–B alloys and with the XPS results of Cartier *et al* [27] on $Fe_{40}Ni_{40}P_{14}B_6$ metallic glasses. On the other hand Tanaka *et al* have observed a drastic shift in the d band by 1 eV. Such a strong d-band shift for Ni_3Si is in contradiction to UPS [28], bremsstrahlung isochromat spectroscopy and XPS results too [29]. Consequently the lowering of the d band in amorphous $Ni_{1-x}P_x$ and Ni_3Si alloys should be much smaller (in the range of a few tenths of an electronvolt); otherwise the d band would completely be filled and $N(E_F)$ would decrease close to zero, which is

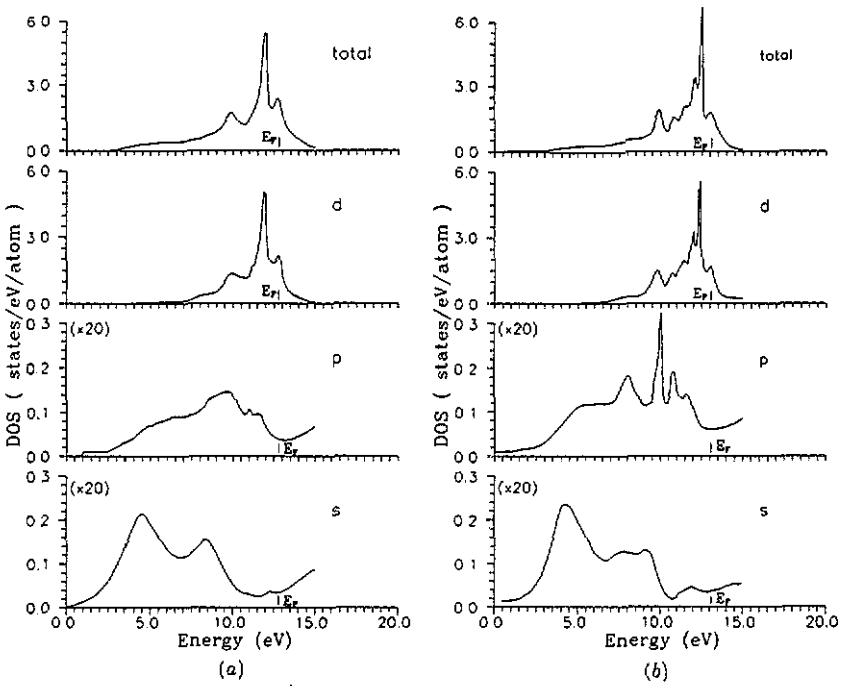

Figure 3. (*a*) The calculated Ni total DOS and partial DOS (s, p, d) of Ni_3P with Ni in the centre of the cluster (MT radius $r_{Ni}^{MT} = r_P^{MT} = 2.363\,15$ au; computational method, cluster LCPA; cluster size, 13 atoms). (*b*) The calculated Ni total DOS and partial DOS (s, p, d) of Ni_3P with Ni in the centre of the cluster (MT radius $r_{Ni}^{MT} = r_P^{MT} = 2.363\,15$ au; computational methods, cluster LCPA; cluster size, 27 atoms).

obviously not true [7]. Meanwhile the small amount of d-band shift also agrees with the calculations performed by Khanna *et al* [11], Ching [9] and Press *et al* [10].

Considering the site selectivity of XES and XAS we have used a two-band model. A site-dependent cluster LCPA method with different cluster sizes has been performed. The DOS of the central atoms of the clusters were determined by this method. The central atoms of the clusters were either Ni or P atoms. The cluster symmetry conforms with the Ni_3P structure [20]. The results of these calculations are presented in figure 3 where the central atom is Ni. With increasing cluster size, the DOS shows much sharper and well characterized features, but the main structures are independent of the cluster size. Therefore, the DOS of the central Ni atom weakly depends on the higher coordination shells in NiP.

Additionally we present the Ni DOS results of the LAPW method in figure 4. The main Ni DOS peak of pure Ni is positioned at -0.5 eV, whereas the corresponding main peak of Ni–P alloy is located at -0.8 eV (figure 3(*b*)).

The characteristic Ni d-band data of metal and alloy are collected in table 5, indicating a Ni d-band shift for Ni_3P with respect to that for pure Ni to higher binding energies by 0.2–0.3 eV.

According to Ching's [9] cluster calculations on amorphous Ni–P, the alloy DOS is due to an average over different kinds of Ni atom with respect to different P neighbours, which causes a smearing (or broadening) of the d DOS. (Ching has shown that, with

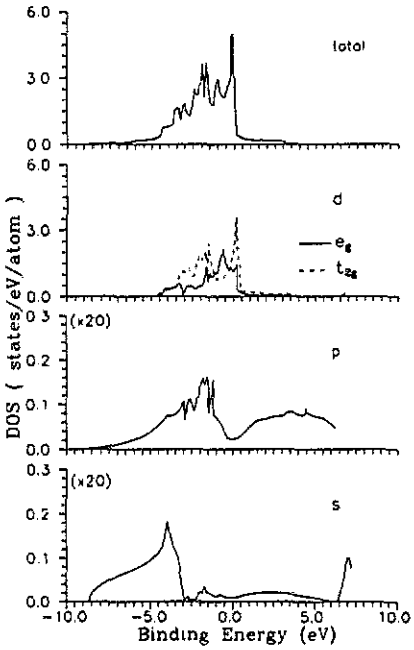

Figure 4. The calculated Ni total DOS and partial DOS (s, p, d) of FCC Ni lattice (MT radius $r_{Ni}^{MT} = r_P^{MT} = 2.35$ au; computational method, LAPW).

Table 5. A few characteristic data for d DOSs of Ni resulting from different calculations for Ni and Ni_3P. $E_{d,max}^{bond}$ is bonding energy of d-DOS^{max} (Δ and δ as in table 3). d DOS^{max} is the maxima of the d DOS. d DOS(E_F) is the d DOS at E_F. HBW is the half-band-width.

	$E_{d,max}^{bond}$ (eV)	d DOS^{max} (states eV^{-1}/atom)	d DOS(E_F) (states eV^{-1}/atom)	HBW (eV)
		Ni		
LAPW FCC	0.1	5.2	4.1	3.0
LAPW BCC	−0.5	8.8	2.8	3.0
[9]	−0.2	4.8	4.0	—
[10]	−0.3	—	—	3.2
XES Ni L_3	−0.7 ± 0.2	—	—	1.7 ± 0.2
		Ni_3P		
Cluster LCPA FCC first shell	−0.8	5.2	1.8	3.4
Cluster LCPA FCC second shell	−1.0	6.3	1.6	3.7
[9]	−1.2	1.0	0.59	4.5
[8]	−1.0	2.5	0.67	3.3
[10]	+0.2	—	—	2.5
XES Ni L_3	−0.9 ± 0.2	—	—	1.7 ± 0.2

increasing numbers of neighbouring P atoms, a stronger Ni d-band shift to higher binding energies is caused.) Consequently the alloy d states are more strongly bonded but are not filled much more than in the pure metal [10, 11].

4.1.2. s band. Despite the difficulties in detecting the s band by XES, Tanaka *et al* [30] found a slight increase in the tail of the Ni L_3 spectrum of $Ni_{80}P_{20}$ at binding energies between −5 and −8 eV. This increase can be interpreted as a shift in the Ni s band to higher binding energies and simultaneously an enhancement in the s DOS at an energy of −8 eV. This interpretation agrees well with our cluster calculations, which predict a new Ni s DOS peak at -8.5 ± 0.2 eV binding energy in Ni_3P (figure 3).

4.2. Density of states around P

4.2.1. s + d band. By alloying, the core level shift of the phosphorus atom is much more pronounced than the corresponding shift of the Ni atom. The P $2p_{1/2,3/2}$ level shift to lower energies has been measured by XPS in the range of 0.4–0.5 eV [25, 31, 32] (the results are summarized in table 4). This shift corresponds to a charge transfer from Ni to P. The observed shifts of the P core levels are much more drastic than the corresponding Ni shifts, because the charge transfer is higher at the (minority) P atom (0.4 e^-) than at the Ni atom (0.1 e^-).

The XES-spectra of the P in Ni–P alloy drastically differ from the corresponding P $L_{2,3}$ spectrum for pure phosphorus [25]. Two effects cause these strong differences.

(i) The alloy P 3s band becomes strongly bonded and localized. Similar phenomena are also observed by XES on the metalloid 3s band in Mo_3Si, ZrSi and Nb_4Si alloys [33] as well as in $CuMoS_8$ [34]. In the Ni–P alloy the P 3s band becomes effectively a 'quasi-core' band with the binding energy of −13.1 eV. The main peak A at 116.5 eV in the P $L_{2,3}$ spectrum is attributed to this band. The localization index calculations [9] also show a strong degree of localization of P 3s.

Fujiwara [35] has calculated the electronic structure of amorphous Fe–P alloys and interpreted the P 3s-electron state as a 'frozen' atomic state. Our cluster calculations on Ni–P are in agreement with this picture (figure 5(*b*)). The P 3s state is localized at the muffin-tin zero energy, which corresponds to −12.7 eV binding energy (table 6). This 3s band is very sharp and well localized at low metalloid concentrations ($0.08 \leqslant x \leqslant 0.26$) but is much more broadened or delocalized in metalloid-rich alloys. Similar dependences have been demonstrated for several silicides [29, 36, 37].

(ii) By alloying, around the P atoms 'new d states' were created, which result from the charge transfer from Ni to P. Experimentally, this interpretation is based on the existence of a new subpeak in the P $L_{2,3}$ spectra (peak B at 127.1 eV). The relative peak intensity, the energy position and the full width at the half-maximum are not significantly dependent on the P concentration in the investigated concentration range. These extra d states around the P atoms are also confirmed by our calculations (table 7). This P d band is close to the Fermi level (theoretical, −1.0 to −1.7 eV; experimental −2.5 eV) and has approximately 3.8 eV bandwidth. These parameters indicate that the Ni d band and the P d band have very similar features; consequently we interpret these two d bands as a common d band [11]. The d states close to the Fermi level in the Ni–P alloy are mainly delocalized as has been obtained by the localization index analysis of Ching [9]. The extended Ni d states overlap with the P p states. From this hybridization some P d states result.

The Si $L_{2,3}$ XES data of Mo_3Si, Nb_4Si and ZrSi show [33] similar peaks as the Ni–P P $L_{2,3}$ subpeak B. These data can also be explained by the d-band assumption in the metalloid site, which is connected by the extended metal d wavefunctions overlapping with the metalloid wavefunctions [29].

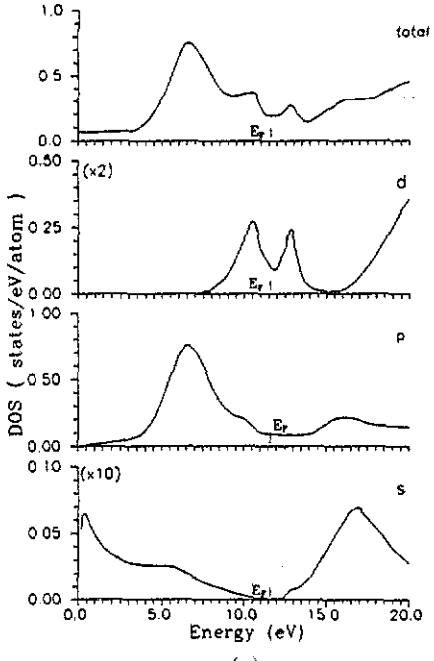

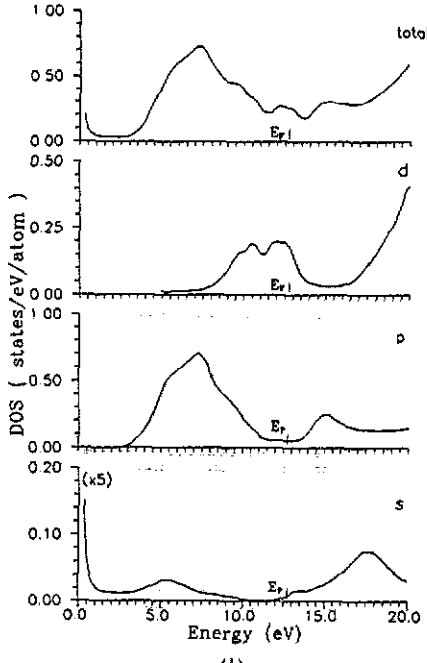

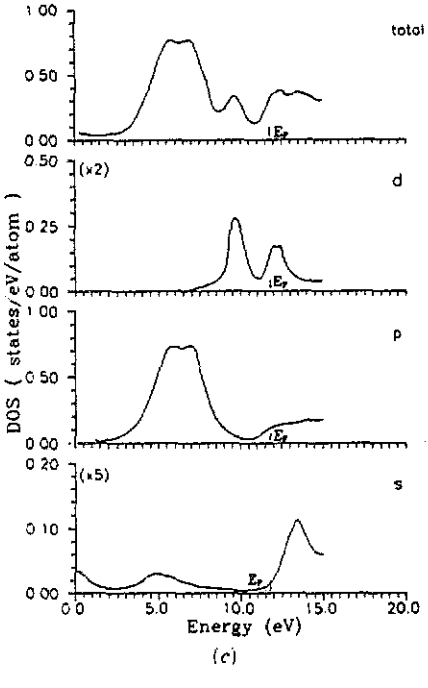

Figure 5. (*a*) The calculated P total DOS and partial DOS (s, p, d) of Ni_3P with P in the centre of the cluster (MT radius $r_{Ni}^{MT} = r_P^{MT} = 2.363\,15$ au; computational method, cluster LCPA; cluster size, 14 atoms). (*b*) The calculated P total DOS and partial DOS (s, p, d) of Ni_3P with P in the centre of the cluster (MT radius) $r_{Ni}^{MT} = r_P^{MT} = 2.363\,15$ au; computational method, cluster LCPA; cluster size, 29 atoms). (*c*) The calculated P total DOS and partial DOS (s, p, d) of FCC NiP lattice (MT radius $r_{Ni}^{MT} = r_P^{MT} = 2.363\,315$ au; computational method, cluster LCPA; cluster size, 19 atoms; two coordination shells).

Goldstein *et al* [39] measured the Al $L_{2,3}$ XES spectra of Ni–Al, which were interpreted by Schwarz *et al* [22] predicting a considerable d DOS on an Al site by an APW band-structure calculation, which supports our proposal well.

Table 6. The binding energies and the maximum of the P 3s DOS in selected Ni–P binary compounds.

	$E^{max}_{s,bond}$ (eV)	3s DOS$^{max a}$ (states eV^{-1}/atom)
Fe_3P [35]	−10.4	3.0
$Ni_{75}P_{25}$ [9]	−14.0	0.4
$Ni_{80}P_{20}$ [9]	−14.5	0.4
$Ni_{85}P_{15}$ [9]	−15.0	0.4
Ni_3P [10]	−8.0	2.8
$Ni_{12}P_5$ [10]	−7.5	2.6
Ni_2P [10]	−8.5	2.4
$Ni_{75}P_{25}$ [8]	−12.0	1.2
Ni_3P cluster LCPA	−12.7	—
UPS (Fe_3P) [45]	−13.5	
XES $Ni_{1-x}P_x$[b]	−13.1	1.0[c]

[a] Normalized for P atom.
[b] No concentration dependence.
[c] Calculated P 3s charge equal to $2e^-$ ($HBW_{eff} = 2$ eV; band shape is approximated by a triangle [35]).

Table 7. Few characteristic data for p and d DOSs of P in Ni–P alloy.

	$E^{bond}_{d,max}$ (eV)	d DOS^{max} (states eV^{-1}/atom)	$E^{bond}_{p,max}$ (eV)	p DOS^{max} (states eV^{-1}/atom)	$E^{hole\ a}_{p,max}$ (eV)
LAPW P in FCC Ni	−1.0	0.12	−5.8	0.68	6.5
LAPW P in BCC Ni	−1.5	0.12	−5.3	0.65	6.0
Ni_3P cluster LCPA (1 shell; 14 atoms)	−1.3	0.22	−5.2	0.71	—
Ni_3P cluster LCPA (2 shells; 29 atoms)	−0.8	0.18	−5.6	0.65	—
FCC $Ni_{75}P_{25}$	−1.7	0.24	−5.4	0.69	—
Ni_3P [9]	—	—	−5.0	0.7	—
$Ni_{80}P_{20}$ [8]	—	—	−6.0	0.5	—
Ni_3P [10]	—	—	−9.0	—	7.0
XES, XAS $Ni_{1-x}P_x$[b]	−2.5 ± 0.3	—	−5.9 ± 0.3	—	6.4 ± 0.5 [31]
XPS [23]	—	—	−6.5 ± 0.5	—	—

[a] Unfilled p band (antibonding band).
[b] No concentration dependence.

In order to determine the effective induced d charge at the P sites, one has to integrate the d DOS up to E_F. From the integration we get 0.31 d electrons per P atom (table 8). In a similar way we obtained a P 3s-electron number of 1.5 e^- in the localized state ('quasi-core band' at −13.1 eV) and 0.1 e^- in the valence band. Therefore, the contribution of the s band to the P $L_{2,3}$ subpeak B is weak (less than 20%; so it can be neglected in first

Table 8. The local DOSs at E_F and the site and symmetry selective charge (Q) distribution in $Ni_{75}P_{25}$.

	[9]	[8]	LAPW	Cluster LCPA	XES	XPS[a]
Ni Q s (electrons)	0.83	—	—	1.1	—	—
Q p (electrons)	0.63	—	—	0.8	—	—
Q d (electrons)	8.33	—	—	8.0	—	—
Q total (electrons)	9.87	10.46	—	9.9	—	—
$N(E_F)$ (states eV^{-1}/atom)	0.53	0.67	—	1.6	—	—
P Q s (electrons)	1.68	—	1.47	2.1	2.0	—
Q p (electrons)	3.70	—	2.19	2.9	3.0	—
Q d (electrons)	—	—	0.31	0.4	0.3	—
Q total (electrons)	5.38	3.55	4.69[c]	5.4	5.3	—
$N(E_F)$ (states eV^{-1}/atom)	0.04	—	0.18	0.2	—	—
$\Delta Q^{P}_{Ni\to P}$[b]	+0.38	−1.45	−0.31	+0.4	+0.3	+0.4

[a] Based on 0.4 eV binding energy shifts of $P_{1/2,3/2}$ (table 4).

[b] Charge transfer per phosphorus atom from Ni to P. Because of charge neutrality, $\Delta Q^{Ni} = \Delta Q^{P}/3$ in $Ni_{75}P_{25}$. (Furthermore the ΔQ^{P} does not depend on the phosphorus concentration in the dilute limit.)

[c] Included 0.72 e^- interstitial charges.

approximation). Using this assumption to determine the P 3s and P 3d charge from the subpeak areas of P $L_{2,3}$ spectra (considering the different contributions of s or d DOS to the $L_{2,3}$ spectra [40, 41]), also 0.3–0.4 P d electrons have been obtained.

The induced 0.3 d electrons around the P atoms in the Ni–P alloy coincide with the value of the transferred 0.3–0.4 electrons.

When amorphous Ni–P alloys are created, a charge transfer from Ni to P takes place, but the number of P 3s and P 3p electrons remains nearly constant. This basic assumption is important with respect to the band-gap theory of strong ferromagnetism developed by Malozemoff *et al* [38].

4.2.2. p band. We have no direct information on the P 1s core-level shift, caused by the charge transfer from Ni to P, but from the XAS data or XES P $K\alpha_{1,2}$ [42] combined with XPS P $2p_{1/2,3/2}$ measurements [31] it can be determined. This shift (0.4–0.5 eV) refers to a small amount of charge transfer from Ni to P too.

The XES P $K\beta$ peak of Ni–P differs strongly from the corresponding peak for pure P [25]. This is due to the strong localization of the P 3p states. The P $K\beta$ spectrum consists of two overlapping subpeaks. Peak A (figure 2) corresponds to the pure P 3p state, whereas subpeak S corresponds to the hybridized p–d state. It is evident from the cluster LCPA (figure 5) or from the LAPW (figure 6) calculation that the d DOS around the P atom (at −2.5 eV) coincides with the subpeak of the P p DOS, which corresponds to the subpeak S of the P $K\beta$ spectra (figure 7(*c*)).

The weak concentration dependence of the P $K\beta$ subpeak S is also an indication for p–d hybridization. The total band half-width is plotted in figure 8 for different P concentrations. This concentration dependence proves a stronger hybridization with increasing number of Ni atoms around the P atom. (In the dilute limit the P atom in the Ni–P alloys have ten to 12 Ni nearest neighbours, while at higher concentrations this

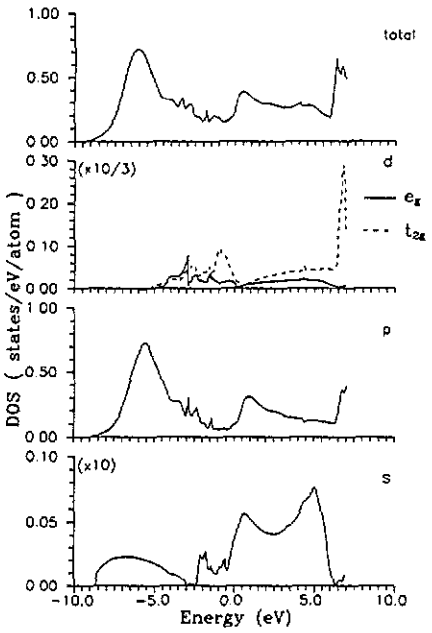

Figure 6. The calculated Ni total DOS and partial DOS (s, p, d) of FCC NiP lattice (MT radius $r_{Ni}^{MT} = r_P^{MT} = 2.35$ au; computational method, LAPW).

number is reduced to nine [20]. In our interpretation the band half-width is increased, because the subpeak S contribution is enhanced (at higher Ni concentrations) as measured directly by Belin *et al* [25], whereas the total number of P 3p electrons is unchanged.

For the P 3p state, the localization is concurrent with hybridization, giving rise to bonding and antibonding p subbands. The Fermi edge is located between these two subbands [26, 29, 43]; therefore the number of P 3p electrons remains at three even at low P concentrations. The energies corresponding to the p DOS maxima are collected in table 7, showing agreement (within 0.5 eV) between the calculated DOS and experimental data. These considerations are valid for both the P Kβ emission and the P K absorption. So the hump at 2149.5 eV in the P K absorption spectra [31] is the antibonding p state at a binding energy of +6.4 eV.

5. Summary

The DOSs around the Ni and P atoms in amorphous Ni–P show the following behaviour with respect to those of the pure components. The Ni d band is shifted away from the Fermi level to higher binding energies by 0.2 eV. The Ni d DOS at E_F is reduced, whereas the number of Ni d holes shows a slight reduction (from 0.6 e^- to 0.5 e^-, which is undetectable within the smeared resolution ($\Delta E = 1.8$ eV) [7]).

The charge transfer is 0.1 electron per Ni atom or 0.3–0.4 electron per P atom transferred from Ni to P (table 8).

The Ni–P P 3s band is split off from the valence band; it becomes localized and strongly bonding at a binding energy of −13.1 eV. This band is occupied with about two electrons. The P 3p band is also strongly bonded and includes nearly three electrons like pure P. The P 3p states are hybridized with the Ni d states and form bonding (−5.9 eV)

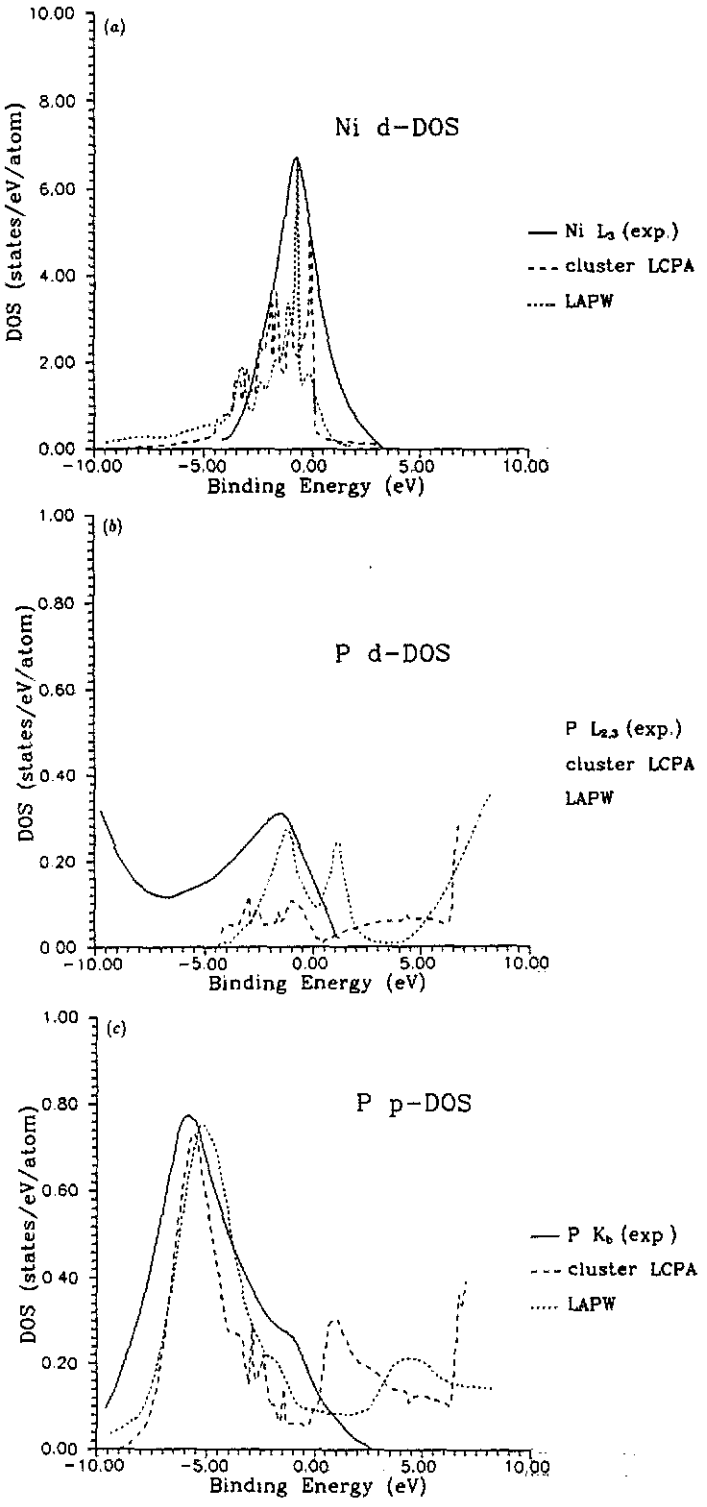

Figure 7. (*a*) The nickel d partial DOS in $Ni_{75}P_{25}$ alloy. (*b*) The phosphorus d partial DOS in $Ni_{75}P_{25}$ alloy. (*c*) The phosphorus p partial DOS in $Ni_{75}P_{25}$ alloy.

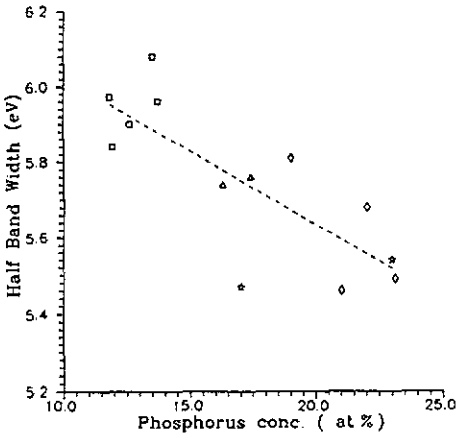

Figure 8. The P Kβ half-band-width dependence on the phosphorus concentration in amorphous Ni–P alloy prepared by electroless (□), electrolytic (*) and rapid quenching (△) techniques.

and antibonding (+6.4 eV) orbitals. The Fermi level is located in the dip between them. Such deep minima exist not only in P 3p but also in P 4s, in P 3d and of course in Ni 3d DOSs close to the Fermi energy as predicted by Terakura [43].

Around the P atoms a new d band is located close to the Fermi level with a binding energy of -2.5 ± 0.5 eV and occupied by 0.3–0.4 electrons.

The interpretation concerning the characteristic metalloid s-band split together with the very strong d-band contribution may be transferred to assignment of the metalloid XES $L_{2,3}$ measurements from different 3d and 4d metalloid-rich silicides [29, 33, 36].

Considering the model calculations, the cluster LCPA methods are much more sensitive to the cluster size than to the cluster symmetries. However, the main features are determined by the first two coordination shells. On the contrary, in the impurity LAPW method the metal (host) DOS strongly depends on the symmetries, whereas the metalloid (impurity) DOS is weakly affected by the host matrix structures. It has been proved that both computational methods can be well fitted to the XES results (figure 7). From this agreement we conclude that the x-ray transition probabilities are only slightly dependent on the binding energy. Furthermore, the radial transition probabilities are weakly dependent also on the symmetries in the metalloid case (the s-band and the d-band transition matrix elements are approximately equal [40]). Only with respect to this approximation can a good fit be obtained.

The smearing in the metal XES spectra is mainly due to lifetime broadening. Therefore, the DOS model calculations yield finer structures than our measurements do. With respect to these considerations, angle- and polarization-resolved XES and XAS [44] can provide us with more detailed metal electron structure information. However, the core broadening of the metalloid XES and the instrumental resolution are both in the range of 0.1 eV, which corresponds to the accuracy of the model calculations. The main changes in electron structures are caused by alloying. They have been well characterized in Ni–P. The electron structure background of easy glass-forming ability of metal–metalloid glasses within a given metalloid concentration range is not yet well understood. The heat evolved upon crystallization is in the range 0.5–0.9 kcal mol^{-1} or 0.02–0.04 eV per atom. Analysis of the amorphous and crystalline electron structure differences requires 0.02 eV accuracy and resolution for experiments and simulations too.

Acknowledgments

One of the authors (JK) would like to thank Professor E Nagy, Professor B Vasvari and E Belin for useful discussion and comments. Thanks are also due to G Nemeth, Z Dankhazi, A Sulakov and A Brajko for their help in the experimental work.

References

[1] Hines W A, Glover K, Clark W G, Kabacoff L T, Modzelewski C U, Hasegawa R and Duwez P 1980 *Phys. Rev.* B **21** 3771
[2] Carini J P, Nagel S R, Varga L K and Smidt T 1983 *Phys. Rev.* B **27** 7589
[3] Tyan Y S and Toth L E 1974 *J. Electron. Mater.* **3** 791
[4] Kuentzler R, Bakonyi I and Lovas A 1985 *Solid State Commun.* **55** 567
[5] Lashmore D S, Benett L H, Scone H E, Gustafson P and Watson R E 1982 *Phys. Rev. Lett.* **48** 1760
[6] Hines W A, Modzelewski C U, Paolino R N and Hasegawa R 1981 *Solid State Commun.* **39** 699
Bakonyi I, Schone H E, Varga L K, Tompa K and Lovas A 1986 *Phys. Rev.* B **33** 5030
[7] Choi M, Pease D M, Hines, W A, Hayes G H, Buidnick J I, Heald S M, Hasegawa R and Schone H E 1985 *Phys. Rev.* B **32** 7670
[8] Jaswal S S 1986 *Phys. Rev.* B **34** 8937
[9] Ching W Y 1986 *Phys. Rev.* B **34** 2080; 1985 *J. Non-Cryst. Solids* **75** 379
[10] Press M R, Khanna S N and Jena P 1987 *Phys. Rev.* B **36** 5446
[11] Khanna S N, Ibrahim A K, McKnight S W and Bansil A 1985 *Solid State Commun.* **55** 223
[12] Stepanyuk V S, Kozlov A A, Katsnelson A A, Farberovich O V, Szasz A and Kojnok J 1990 *Fiz. Tverd. Tela* **32** 146 (in Russian)
Stepanyuk V S, Katsnelson A A, Kozlov A A, Farberovich O V, Szasz A and Kojnok J 1991 *Phys. Status Solidi* b **163** 139
[13] The RSM-500 type instrument was equipped with a blazed 'echelette' diffraction grating coated with gold, with 600 grooves mm^{-1} and a Rowland radius of 2 m. The detector was a secondary-emission multiplier with a KCl photocathode. The higher-order diffractions were suppressed with the aid of a filter mirror covered with polystyrene.
Szasz A, Kojnok J and Belin E 1987 *Solid State Commun.* **64** 775
Lukirskii A P, Britov I A and Koniak N I 1967 *X-ray Analysis Mashinostroenie Leningrad* No 2, p 4 (in Russian)
[14] The SARF-1 type of fluorescence crystal spectrometer has a 500 mm bent radius. The $10\bar{1}0$ beryl and the $10\bar{1}1$ quartz crystal are used in first-order reflection for Ni $L_{2,3}$ and P $K\beta$ measurements, respectively. Further the fourth order of a $10\bar{1}1$ quartz crystal was used in the Ni $K\beta$ case. The detector was an Ar–CH_4 flow counter.
Britov I A, Obolenskii E A, Goldenberg M S, Rabinovich L G and Antoeva T M 1983 *Prib. Tekh. Eksp.* **1** 288 (in Russian)
[15] Szasz A, Kojnok J, Kertesz L, Paal Z and Hegedus Z 1984 *Thin Solid Films* **116** 279
[16] The P concentrations were determined with a Phillips PW 1540 type of x-ray fluorescence system equipped with a pentaerythritol crystal. The concentrations were calibrated using a crystalline $Ni_{80}P_{20}$ alloy. The Ni $K\alpha$ were measured in fifth order, and the P $K\alpha$ in first order; the intensity ratio was 18.1. (The detector was an Ar–CH_4 flow counter; the x-ray emission was excited by a 30 kV, 30 mA W anode.)
[17] Vasvari B, Mark G and Lahdeniemi M 1985 *Desy Jahresbericht* (Hamburg: H Burg Druck) p 138
Vasvari B and Mark G 1987 *Proc. 5th Int. Conf. on Rapidly Quenched Metals* (ed S Steeb and H Warlimont (Amsterdam: North-Holland) p 991
[18] Koelling D and Arbman G J 1975 *J. Phys. F: Met. Phys.* **5** 2043
Padlonezky R, Zeller R and Dederichs P H 1980 *Phys. Rev.* B **22** 5777
Stepanyuk V S, Szasz A, Katsnelson A A, Kozlov A and Farberovich O V 1990 *Z. Phys.* B **81** 391
Stepanjuk V S, Szasz A, Katsnelson A A, Grigorenko B and Farberovich O N 1990 *Phys. Status Solidi* b **160** 219
[19] Moruzzi V L, Janak J F and Williams A R 1978 *Calculated Electronic Structures of Metals* (New York: Pergamon) p 188
[20] Benett L H, Long G G, Kuriyama M and Goldman A I 1986 *Structure and Bonding in Noncrystalline Solids* ed G E Walraffen (New York: Plenum) p 385

[21] Weber T A and Stillinger F H 1985 *Phys. Rev.* B **32** 5402
[22] Schwarz K, Mohn P and Novotny M 1981 *Inner-Shell and X-ray Physics of Atoms and Solids* ed D J Fabian, H Kleinpoppen and L M Watson (London: Plenum) p 631
[23] Amamou A, Aliaga-Guerra D, Panissod P, Krill G and Kuentzler R 1980 *J. Physique Coll.* **41** C8 396
[24] Belin E 1985 unpublished data
[25] Belin E, Traverse A, Szasz A and Machizaud F 1987 *J. Phys. F: Met. Phys.* **17** 1913
[26] Tanaka K, Saito T, Suzuki K and Hasegawa R 1985 *Phys. Rev.* B **32** 6853
[27] Cartier E, Baer Y, Liard M and Guntherhodt H J 1980 *J. Phys. F: Met. Phys.* **10** L21
[28] Franciosi A, Weaver J H and Schmidt F A 1982 *Phys. Rev.* B **26** 546
[29] Sarma D D, Speier W, Zeller R, van Leuken E, de Groot R A and Fuggle J C 1990 *J. Phys.: Condens. Matter* **1** 9131
[30] Tanaka K, Yoshino M and Suzuki K 1982 *J. Phys. Soc. Japan* **51** 3882
[31] Belin E, Bonelle C, Zuckerman S and Machizaud F 1984 *J. Phys. F: Met. Phys.* **14** 625
[32] Chen N, Feng P and Sun J 1985 *Rapidly Quenched Metals* ed S Steeb (Amsterdam: Elsevier) p 999
[33] Sulakov A S, Zimkina T M, Fomichev V A and Nespor V C 1974 *Fiz. Tverd. Tela.* **16** 401 (in Russian); 1977 *Izv. Akad. Nauk.* **41** 216 (in Russian)
[34] Kurmaev E Z, Yarmoshenko J, Nyholm R, Martensson N and Jarborg T 1981 *Solid State Commun.* **37** 647
[35] Fujiwara T 1982 *J. Phys. F: Met. Phys.* **12** 661
[36] Speier W, Kumar L, de Groot R A and Fuggle J C 1990 *J. Phys.: Condens. Matter* **1** 9117
[37] Weaver J H, Moruzzi V L and Schmidt F A 1981 *Phys. Rev.* B **23** 2916
[38] Malozemoff A P, Williams A R and Moruzzi N L 1984 *Phys. Rev.* B **29** 1620
[39] Goldstein H E, Pfliegl R and Kirchmayr H 1981 *Inner-Shell and X-ray Physics of Atoms and Solids* ed D J Fabian, H Kleinpoppen and L M Watson (London: Plenum) p 635
[40] $I(E)_{L_{2,3}} \sim E^3[M_s^2(2p, E - E_{2p}^b)N_s(E) + \ldots \tfrac{2}{3}M_d^2(2p, E - E_{2p}^b)N_d(E)]$
where M_s^2 is the radial transition probability for the $2p \rightarrow 3s$ (valence band) transition, M_d^2 is the radial transition probability for the $2p \rightarrow 3d$ (valence band) transition, $N_s(E)$ and $N_d(E)$ are the s and d DOSs, respectively, and E_{2p}^b is the binding energy of the $2p_{3/2}$ or $2p_{1/2}$ levels (see, e.g., [22]). We have no direct data on M_s^2 or M_p^2 for phosphorus in Ni–P alloy, which can only be estimated. In the case of Fe–Al alloy, Swarz *et al* [41] have calculated these partial transition probabilities for Fe and Al too. They get the following relations:

$$\tfrac{2}{3}M_{d,Fe}^2 \gg M_{s,Fe}^2 \qquad \tfrac{2}{3}M_{d,Al}^2 \ll M_{s,Al}^2.$$

In our calculations we use the following reasonable approximation for Ni–P alloys:

$$\tfrac{2}{3}M_{d,Ni}^2 \gg M_{s,Ni}^2 \qquad \tfrac{2}{3}M_{d,P}^2 = M_{s,P}^2$$

[41] Swarz K, Neckel A and Nordgreen J 1979 *J. Phys. F: Met. Phys.* **9** 2509
[42] $E_{Ni\text{-}P.PK\alpha} - E_{pure\,P.PK\alpha} = -0.1$ eV [31]
[43] Terakura K 1976 *J. Phys. F: Met. Phys.* **6** 1385; 1977 *Physica* B **91** 162
[44] Hayasi Y, Takahashi T, Asahina H, Sagawa T, Morita A and Shirotani I 1984 *Phys. Rev.* B **30** 1891
[45] Amamou A and Krill G 1980 *Solid State Commun.* **33** 1087
[46] Wagner C D 1978 *Handbook of XPS* (Eden Prairie, MN: Perkin–Elmer)
[47] This work
[48] Fomichev V A, Zimkina T M, Rudnov A V and Nemnonov S A 1973 *Band Structure Spectroscopy of Metals and Alloys* ed D J Fabian and L W Watson (London: Academic) p 268
[49] Wiech G 1968 *Z. Phys.* **216** 472
[50] Fomichev V A 1968 *Sov. Phys.–Solid State* **9** 2398
[51] Nagel D J 1973 *Band Structure Spectroscopy of Metals and Alloys* ed D J Fabian and L W Watson (London: Academic) p 467
[52] Keski-Rahkonen O and Krause M O 1974 *At. Data Nucl. Data Tables* **14** 139
[53] Chun H U and Klein H 1978 *Japan. J. Appl. Phys.* **17** Suppl. 17–2 141
[54] Vergand V 1987 *J. Physique* **12** C9 923
[55] van der Laan G, Zaanan J, Sawatzky G A, Karnatak R and Esteva J-M 1986 *Phys. Rev.* B **33** 4253
[56] Belin E, Bonelle C, Flechon J and Machizaud F 1980 *J. Non-Cryst. Solids* **41** 219
[57] Belin E, Senemaud C and Zuckerman S 1982 *Solid State Commun.* **44** 413
[58] Ulmer K 1978 *Japan. J. Appl. Phys.* **17** Suppl. 17–2 154
[59] Kunz C 1973 *Band Structure Spectroscopy of Metals and Alloys* ed D J Fabian and L W Watson (London: Academic) p 504